ADVANCED HEALTHCARE MATERIALS
www.advhealthmat.de

Multifunctional STING-Activating Mn_3O_4@Au-dsDNA/DOX Nanoparticle for Antitumor Immunotherapy

*Min Zhou, Xiaoyu Wang, Shichao Lin, Yuan Cheng, Sheng Zhao, Junshu Lin, Zhuoyao Fang, Zhangping Lou, Li Qin, and Hui Wei**

The promise of immunotherapy for cancer therapy has not been fully fulfilled because portions of tumors are immunosuppressive. To tackle this challenge, the initiation of immune system by stimulator of interferon genes (STING) pathway is explored and multifunctional STING-activating nanoparticles are rationally designed for synergistic antitumor therapy. The STING-activating nanoparticles have a formulation of Mn_3O_4@Au-dsDNA/DOX, where dsDNA is used to activate STING for immunotherapy and doxorubicin (DOX) is chosen as a model drug for chemotherapy. The STING-mediated immunity is activated, inducing interferon-β (IFN-β) production, increasing T cell priming, and enhancing effector T cell infiltration. Combined with chemotherapy, STING-mediated immunotherapy shows good antitumor efficacy by inhibiting tumor growth and prolonging survival rate in vivo. The promise of cancer immunotherapy can be fulfilled by combining novel antitumor immunity with innovative nanotechnology, and chemotherapy and targeted therapies.

1. Introduction

Immunotherapy has shown enormous promise in cancer treatment, as evidenced by the recent success of immune-checkpoint blockade therapy even for advanced-stage tumors.[1–12] But only certain percentage of patients responded to this type of immunotherapy. This limitation is largely attributed to the fact that a large portion of tumors are immunosuppressive, characterized by low T cell infiltration.[13,14] To enable immunotherapy for immunosuppressive tumors, numerous emerging strategies have been developed, such as chimeric antigen receptor-redirected T lymphocytes (CAR T cells) and tumor-infiltrating T lymphocytes (TIL T cells) therapies.[15,16] However, these therapies depend on sophisticated cell engineering and are inefficient due to the side effects. Therefore, new strategies to activate antitumor immunity are highly needed. Since the initiation of the innate immune system is also significant to improve cancer immunotherapy, we envisioned that an effective innate immune activating strategy would benefit the immunotherapy.

Stimulator of interferon genes (STING)-mediated stimulation of innate immune has attracted lots of attention because of its newly discovered role in antitumor immunity.[17–21] Cytosolic double-stranded DNA (dsDNA), both exogenous and endogenous, is sensed by cyclic guanosine monophosphate–adenosine monophosphate synthase (cGAS) and converted into cyclic guanosine monophosphate–adenosine monophosphate (cGAMP), which then binds to STING.[18,22] Upon cGAMP binding, STING is activated by dimerization and subsequently triggers a signaling cascade reaction to produce type I interferons (IFNs, particularly IFN-β).[19,20] IFN-β is critical for activation of antigen-presenting cells (e.g., dendritic cells) and then for T cell priming as well as T cell infiltration (**Scheme 1**).

Although recent studies demonstrated that the cyclic dinucleotides (CDNs, including cGAMP and analogues) are potent therapeutic candidates for activating antitumor immunity, the synthesis (especially the nonhydrolyzable ones) and systemic delivery of CDNs are still very challenging because of their complicated structures, negative charges, and feasible hydrolysis.[23–25] These challenges may hamper their further application. Compared with CDNs, dsDNA is easier to be synthesized and more

M. Zhou, Dr. X. Wang, S. Lin, Dr. Y. Cheng, S. Zhao, J. Lin, Z. Lou, L. Qin, Prof. H. Wei
College of Engineering and Applied Sciences
Nanjing National Laboratory of Microstructures
Jiangsu Key Laboratory of Artificial Functional Materials
Nanjing University
Nanjing, Jiangsu 210093, China
E-mail: weihui@nju.edu.cn

J. Lin
Department of Biomaterials
College of Materials
Xiamen University
Xiamen, Fujian 361005, China

Z. Fang
State Key Laboratory of Pollution Control and Resource Reuse
School of the Environment
Nanjing University
Nanjing, Jiangsu 210023, China

Prof. H. Wei
State Key Laboratory of Analytical Chemistry for Life Science
State Key Laboratory of Coordination Chemistry
School of Chemistry and Chemical Engineering
Nanjing University
Nanjing, Jiangsu 210023, China

The ORCID identification number(s) for the author(s) of this article can be found under https://doi.org/10.1002/adhm.202000064

DOI: 10.1002/adhm.202000064

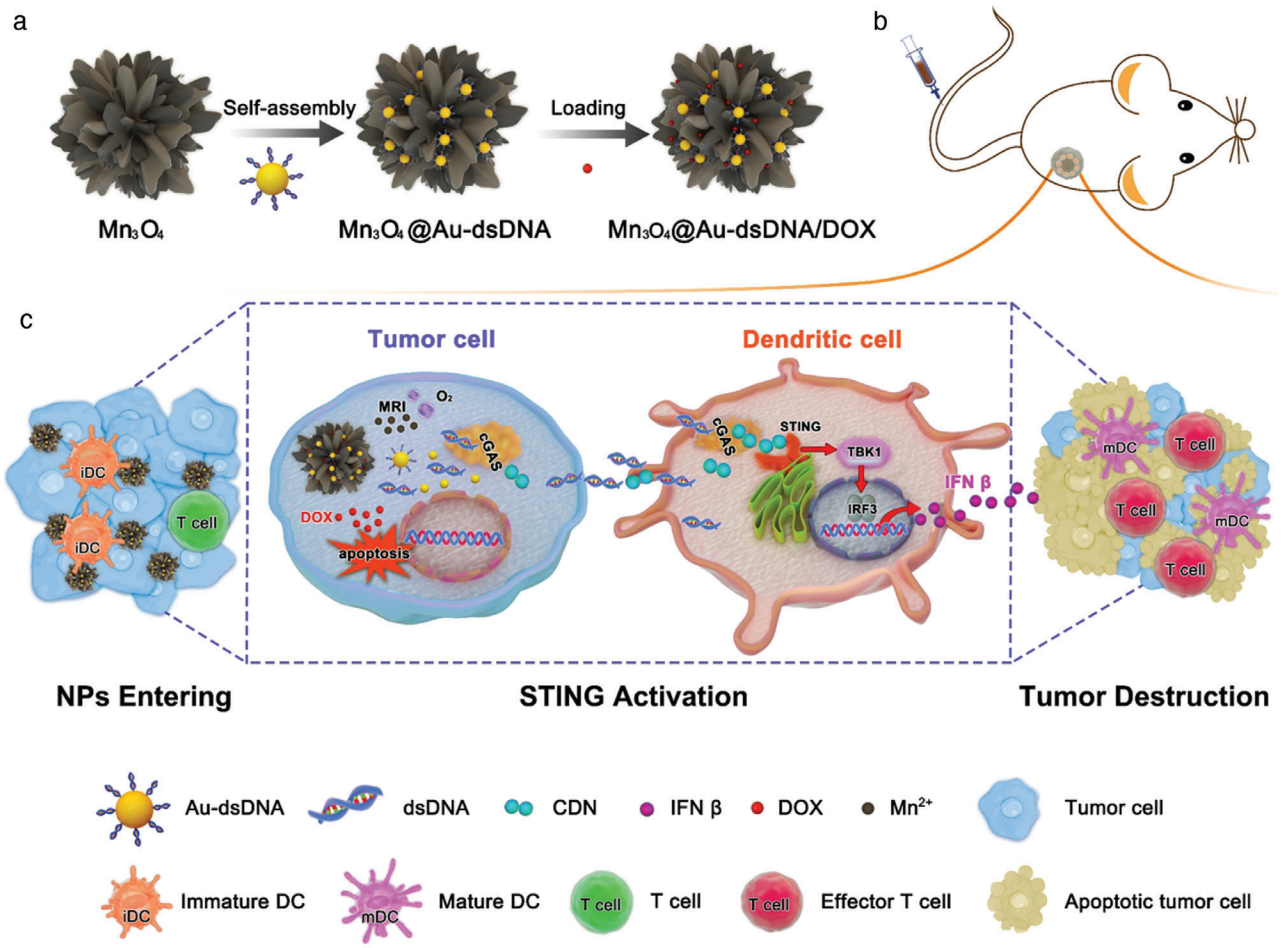

Scheme 1. Design and synthesis of multifunctional STING-activating NPs for synergistic antitumor therapy. a) Schematic showing design and synthesis of STING-activating Mn_3O_4@Au-dsDNA/DOX NPs. b) Tumor-bearing mice were injected intravenously with the designed NPs for therapy. c) MfAND for synergistic dsDNA-mediated immunotherapy and DOX-mediated chemotherapy.

resistant to hydrolysis. In this regard, dsDNA could be an alternative candidate for activating STING-mediated antitumor immunity.[26] However, dsDNA can be digested by DNases. Therefore, further chemical modifications are needed to improve the resistance of dsDNA against DNases.[26] Such modifications are not only laborious but also increase the cost. Moreover, to our knowledge, the systemic delivery of dsDNA into solid tumors for the STING-mediated immunotherapy has not yet been achieved.

On the other hand, emerging evidence showed that the combination of immunotherapy and chemotherapy could synergistically enhance the therapeutic efficacy.[27–29] For example, synthetic high-density lipoprotein nanodiscs were developed to co-deliver immunostimulatory CpG oligonucleotides and docetaxel to treat glioblastoma.[30] However, the co-delivery of an immune activator and a chemotherapeutic drug remains a challenge, which, if achieved, would benefit the systemic delivery and ensure the co-localization of the two therapeutics for better efficacy.

To fill these gaps, herein we designed a multifunctional STING-activating nanoparticle (NP) with the formulation of Mn_3O_4@Au-dsDNA/DOX (MfAND) for synergistic antitumor therapy, which could not only deliver dsDNA into solid tumors for the STING-mediated immunotherapy but also coordinate with chemotherapy (Scheme 1). The MfAND NP was rationally designed as follows: 59 bp poly(dA):poly(dT) was chosen as the dsDNA to activate STING for immunotherapy and DOX was chosen as a model drug for chemotherapy, respectively. The poly(dT) single-stranded DNA (ssDNA) was pre-conjugated onto AuNP via Au-S bond and then annealed with complementary poly(dA) ssDNA to form Au-dsDNA (i.e., AN). The AN and DOX were then co-assembled onto the Mn_3O_4 nanoflower (i.e., Mf) to form the multifunctional STING-activating NP (i.e., MfAND). Importantly, the Mf could be decomposed easily in the tumor cells, leading to the release of the dsDNA and DOX for therapy. Moreover, the released Mn^{2+} ions could be served as a contrast agent for magnetic resonance imaging (MRI). The MRI imaging property of the Mf would allow us to evaluate the accumulation of NPs in tumors.

2. Results and Discussion

AuNPs were prepared via the citrate reduction method[31] and were confirmed by transmission electron microscopy (TEM) imaging (Figure S1a, Supporting Information). The AN was

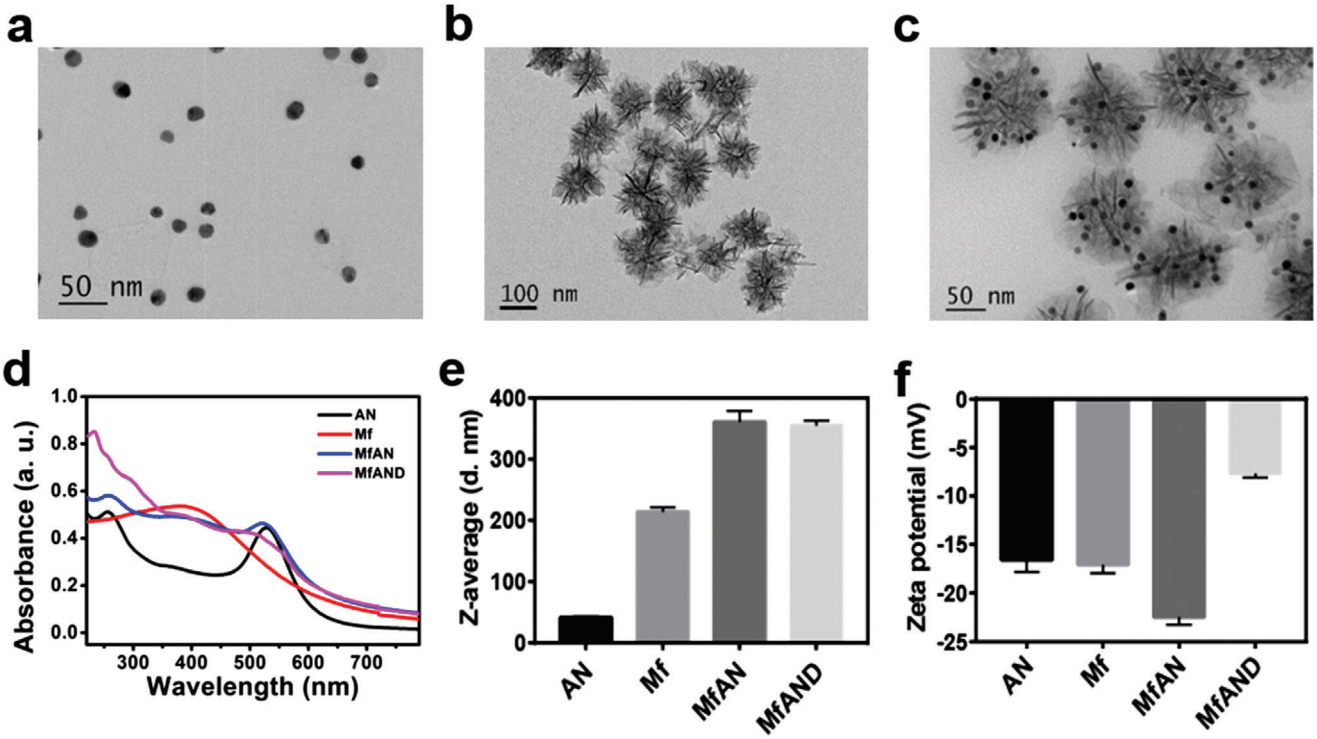

Figure 1. Characterization of the designed NPs. TEM images of a) AN, b) Mf, and c) MfAN. d) UV–vis absorption spectra, e) Z-average diameter, and f) zeta-potential of AN, Mf, MfAN, and MfAND. Each error bar shows the standard deviation of three independent measurements.

prepared in two steps: the conjugation of a thiolated ssDNA (i.e., 59-nt poly(dT) with thiol modification at the 3′ end) onto AuNPs and then annealing with the complementary ssDNA (i.e., 59-nt poly(dA)). The formation of AN was confirmed by TEM imaging (**Figure 1**a) as well as UV–vis absorption spectroscopy and gel analysis (Figure 1d; Figure S1b, Supporting Information). Monodispersed Mf was synthesized according to a previous method[32,33] and was confirmed by TEM and scanning electron microscopy (SEM) imaging (Figure 1b; Figure S2a, Supporting Information). The crystalline nature of Mf was characterized by powder X-ray diffraction, which revealed a structure of tetragonal hausmannite (JCPDS 24-0734) (Figure S2b, Supporting Information). The AN was then assembled onto the Mf via a noncovalent attachment strategy[34] to form Mn_3O_4@Au-dsDNA (MfAN). A typical TEM image in Figure 1c showed the successful assembly of MfAN. Notably, the ratio of AN to Mf in the MfAN could be facilely tuned (Figure S3, Supporting Information). Moreover, when we changed the ratio of AN to Mf, well-dispersed morphology was observed even the ratio was up to 20:1 (weight/weight). Finally, DOX was loaded on the MfAN to obtain the MfAND. The successful loading of DOX was verified by UV–vis absorption spectroscopy (Figure 1d). The loading efficiency of DOX was evaluated by a fluorescent assay (Figure S4, Supporting Information). The average hydrodynamic sizes of AN, Mf, MfAN, and MfAND were about 42 ± 2, 214 ± 7, 361 ± 18, and 354 ± 8 nm, respectively (Figure 1e). The corresponding zeta-potentials were –16.7, –17.1, –22.5, and –7.7 mV, respectively (Figure 1f).

The cytotoxicity of the above NPs was evaluated by using the CCK-8 assay. As shown in **Figure 2**a, as high as 60 μg mL^{-1} AN (AuNPs' concentration) showed negligible cytotoxicity towards B16F10 cells, demonstrating its good biocompatibility. For Mf, as high as 10 μg mL^{-1} Mf exhibited negligible cytotoxicity, while the Mf of higher concentration (≥20 μg mL^{-1}) showed dose-dependent cytotoxicity (Figure 2b). Based on the above cytotoxicity assay, 5 μg mL^{-1} Mf were selected for the following cell studies. We further evaluated the cytotoxicity of the assembled MfAN NPs, which had 5 μg mL^{-1} Mf but varying AN concentration. All the MfAN NPs showed satisfactory cell viability towards B16F10 cells (Figure 2c). We also evaluated the cytotoxicity of MfD and MfAND NPs. As shown in Figure 2d, compared with other NPs, both MfD and MfAND NPs showed obvious cytotoxicity towards B16F10 cells, which were attributed to the loaded DOX (Figure S5, Supporting Information).

To understand the potential cellular internalization process and release mechanisms, we have performed the following studies. First, to support the NPs entry in Scheme 1, we employed TEM to image the MfAN NPs when co-cultured with cells at different time points. Figure S6a, Supporting Information, suggested that the intact MfAN NPs were observed in cells at early stage; then MfAN NPs captured by endosome were observed in Figure S6b, Supporting Information; later MfAN NPs were released from endosome and disassembled as Figure S6c, Supporting Information; no intact MfAN structure were seen in the cell and only Au NPs were imaged in later stage, indicating the degradation of MfAN NPs in cellular environment (Figure S6d, Supporting Information). Meanwhile the intact structure of MfAN NPs outside of the cells was observed (Figure S7, Supporting Information), which further corroborated that MfAN was degraded within the cellular environment. Then, we used the DOX release as an example to investigate the payload-release mechanism from

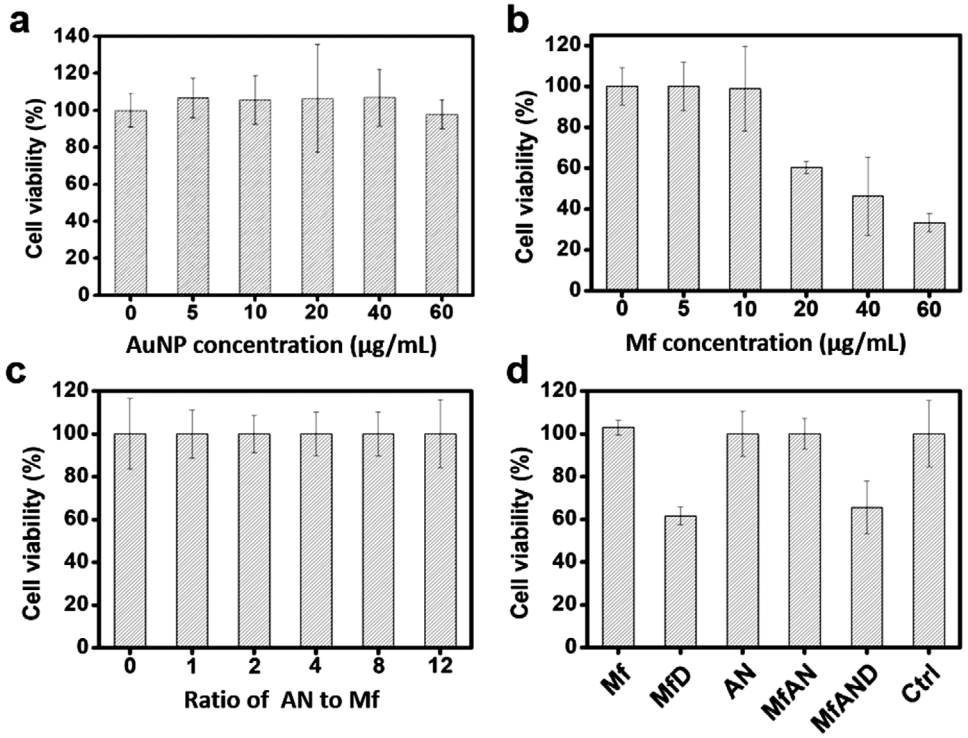

Figure 2. Cell viability of different treatments. a,b) B16F10 cell viability of different AN and Mf concentrations. Concentrations as 0, 5, 10, 20, 40, and 60 μg mL^{-1}. c) B16F10 cell viability of different ratio of AN and Mf. Mf concentration was kept as 5 μg mL^{-1}. d) B16F10 cell viability of Mf (Mn_3O_4: 5 μg mL^{-1}), MfD (Mn_3O_4: 5 μg mL^{-1}, DOX: 125×10^{-9} M), AN (dsDNA: 6 μg mL^{-1}), MfAN (Mn_3O_4: 5 μg mL^{-1}, dsDNA: 6 μg mL^{-1}), MfAND (Mn_3O_4: 5 μg mL^{-1}, dsDNA: 6 μg mL^{-1}, DOX: 125×10^{-9} M), and Ctrl (PBS). Each error bar shows the standard deviation of four independent measurements.

the assembled NPs under different tumor microenvironments, such as low pH and high glutathione (GSH) concentration. We tested the different pH of 7.4, 6.5, and 5.5, and different GSH concentrations of 0×10^{-3}, 1×10^{-3}, 2×10^{-3}, and 5×10^{-3} M. As shown in Figure S8, Supporting Information, although both low pH and high concentration of GSH induced the release of DOX, higher GSH concentration played a more pronounced role in DOX releasing.

After the cytotoxicity analysis, we then studied the effects of the designed NPs on the activation of STING pathway in vitro. Considering that IFN-β is a vital cytokine in the STING signal pathway, we determined the NPs-stimulated production of IFN-β at the cellular level. First, we measured the production of IFN-β in the NPs-treated B16F10 cancer cells. As shown in **Figure 3**b, all groups induced negligible level of IFN-β, suggesting that the STING pathway in B16F10 cells might be suppressed. It is known that the STING pathway could be used to initiate the innate immune system against virus, so we detected the antivirus activity of B16F10 cells. As shown in Figure S9a, Supporting Information, B16F10 cells had negligible antivirus activity. This was another indication that the STING pathway in B16F10 cells was inhibited. These two results also agreed well with previous reports that the STING pathway in cancer cells was suppressed.[35,36] Now that IFN-β is critical for the activation of antigen presenting cells (e.g., macrophages and dendritic cells), here we chose RAW 264.7 macrophage as a model to investigate the activation of STING pathway in vitro (Figure 3a). Once the macrophages phagocytose these dying cancer cells, the released STING activators (such as dsDNA and CDNs) from the engulfed cancer cells stimulate the production of IFN-β. We measured the expression of IFN-β in RAW 264.7 macrophages after engulfing different NPs-treated dying cancer cells. As shown in Figure 3c, all the NPs induced the production of IFN-β. Moreover, the NPs containing dsDNA induced higher level of IFN-β than those without dsDNA. Notably, the control group without NPs treatment also induced the production of IFN-β, which could be attributed to the limited endogenous dsDNA from the dying cancer cells. The Mf and MfD NPs did not show significant differences compared with the control group, suggesting that Mf and DOX were not effective STING activators. The higher level of IFN-β induced by the NPs containing dsDNA could be attributed to the higher immunogenicity of exogenous dsDNA, which was consistent with previous reports.[37] Interestingly, MfAND showed better efficacy than the other two dsDNA-contained NPs (i.e., AN and MfAN). This was probably owing to the synergistic effects of DOX-mediated chemotherapy and dsDNA-stimulated immunotherapy.

After demonstrating the immunostimulating efficacy in vitro, we next investigated the antitumor activity of the NPs in vivo. Here, we chose B16F10 tumor-bearing C57BL/6 mice as the tumor model. After tumor formation, the mice were randomized into six groups and treated with different NPs by intravenous injection. The results are summarized in **Figure 4**a,b. All the three NPs containing dsDNA (i.e., AN, MfAN, and MfAND) significantly inhibited the tumor growth, suggesting that dsDNA delivered into tumors could activate the STING pathway for antitumor immunity. MfD significantly inhibited the tumor growth,

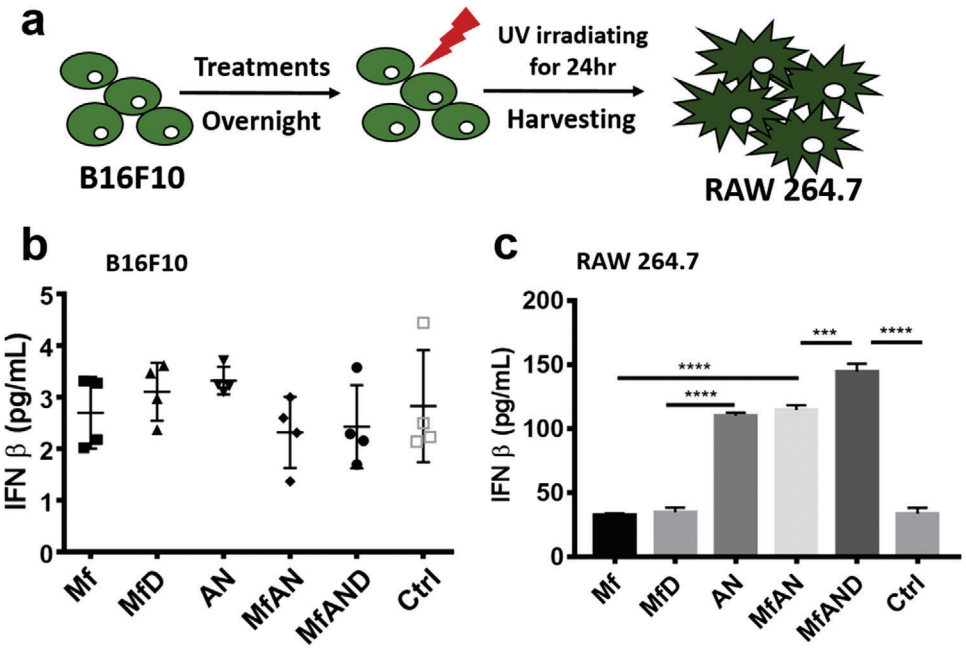

Figure 3. Detection of STING-mediated IFN-β production. a) Scheme of detecting STING-mediated IFN-β production. b,c) Level of IFN-β expression in NPs-treated B16F10 cells and RAW 264.7 cells, respectively. Indicated treatments: Mf (Mn_3O_4, 5 μg mL^{-1}), MfD (Mn_3O_4: 5 μg mL^{-1}, DOX: 125 × 10^{-9} M), AN (dsDNA: 6 μg mL^{-1}), MfAN (Mn_3O_4: 5 μg mL^{-1}, dsDNA: 6 μg mL^{-1}), MfAND (Mn_3O_4: 5 μg mL^{-1}, dsDNA: 6 μg mL^{-1}, DOX: 125 × 10^{-9} M), and Ctrl (PBS). Each error bar shows the standard deviation of four independent measurements. Data were analyzed with ordinary one-way ANOVA. ****$p < 0.0001$.

which was originated from the antitumor activity of DOX. Moreover, the average tumor volume in MfAND-treated group was the smallest, only one sixth of the control group at sacrifice. The MfAND-treated group containing both dsDNA and DOX exhibited the most potent antitumor activity compared with the other two dsDNA-contained NPs (i.e., AN and MfAN) and the DOX-contained NP (i.e., MfD). The enhanced efficacy of MfAND could be attributed to the synergistic effects of DOX-mediated chemotherapy and dsDNA-stimulated immunotherapy.

With the potent antitumor activities, we also explored whether the STING-activating NPs could benefit the survival rate. C57BL/6 mice were transplanted intradermally with B16F10 cells, and then were treated with the different NPs at days 7, 9, and 11. Mice were sacrificed when the tumor volume reached 1500 mm^3. As the survival curves shown in Figure 4c, all the three dsDNA-contained NPs significantly prolonged the mice survival time and the MfAND showed the best outcome as long as 60 days.

Notably, our NPs were injected intravenously while the previous phosphorothioate-modified dsDNA as a STING activator was administrated intratumorally.[26] The intravenous injection would be more feasible and applicable to broader patients. The intravenous injection was enabled by the NPs' tumor accumulation via enhanced permeability and retention (EPR) effect. The succesful accumulation of the NPs in the tumor sites was confirmed by the MRI imaging and inductively coupled plasma (ICP) measurements (Figures S10 and S11, Supporting Information). It should also be noted that all the NPs with our doses showed no signs of toxicity in vivo, as demonstrated by neither significant change in body weight (Figure S12, Supporting Information) nor obvious physiopathological changes in major organs (Figure S13, Supporting Information).

To demonstrate that the antitumor property of the dsDNA-contained NPs was originated from STING activation, we monitored the level of IFN-β in the peripheral blood because IFN-β is a distinctive cytokine in STING pathway (Figure 4d,e). The level of IFN-β changes over time, which is generally detectable at 2–9 h after treatments.[38,39] As shown in Figure 4d, the level of IFN-β was not detectable at 3 h for all the NPs. However, IFN-β was detected for the dsDNA-contained NPs at 6 h (Figure 4e), which confirmed our assumption that exogenous dsDNA could activate the STING pathway in vivo.

Tumor necrosis factor alpha (TNF-α), another important cytokine participating in tumorigenesis inhibition, is related to the antitumor ability.[39,40] Here, we detected the TNF-α in the peripheral blood. As shown in Figure 4f, all NPs-treated groups showed the enhanced production of TNF-α. Phosphate-buffered saline (PBS) as the control group had the lowest TNF-α and followed by Mf, AN, and MfAN. MfAND group exhibited the highest production of TNF-α. The trend of TNF-α production matched well with the tumor inhibition efficacy.

As Scheme 1 shows, T cell priming and infiltration is the advanced step in STING-mediated immunotherapy. Therefore, we evaluated the level of effector T cells in spleens after the NPs treatment by flow cytometry. As shown in **Figure 5**a,b, effector T cells in MfAND group exhibited the highest levels as 14.5% CD4$^+$ cells and 9.11% CD8$^+$ cells, respectively. This was consistent with the highest antitumor effect of MfAND. After analyzing the phenotypes of T cells in spleen, we also evaluated the infiltration of effector T cells in resected tumor by using

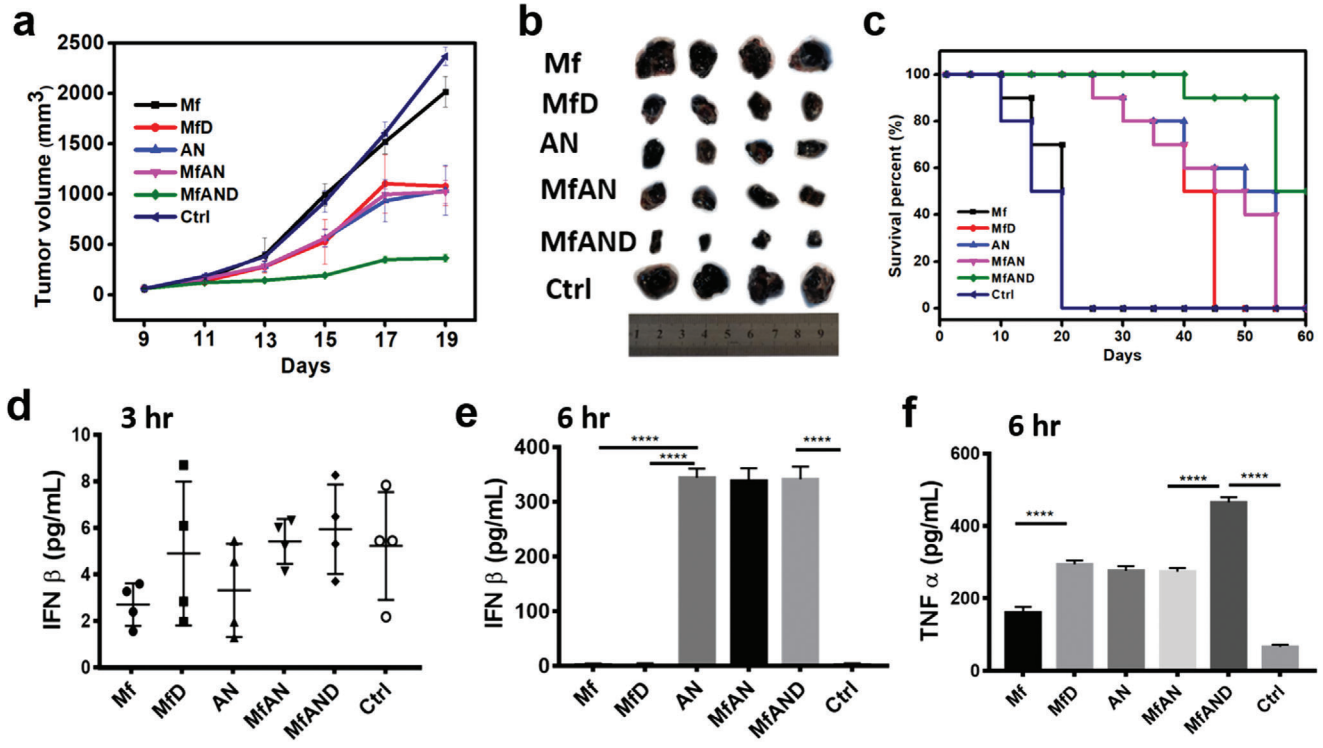

Figure 4. Antitumor effect of the NPs in vivo. a) Tumor volume changes and b) corresponding tumor images of the indicated treatments. c) Survival curves of the indicated treatments. d,e) Level of IFN-β in peripheral blood after indicated treatments at 3 and 6 h, respectively. f) Level of TNF-α in peripheral blood after indicated treatments. Indicated treatments: Mf (Mn_3O_4, 5 mg kg^{-1}), MfD (Mn_3O_4: 5 mg kg^{-1}, DOX: 6 mg kg^{-1}), AN (dsDNA: 10 μg kg^{-1}), MfAN (Mn_3O_4: 5 mg kg^{-1}, dsDNA: 10 μg kg^{-1}), MfAND (Mn_3O_4: 5 mg kg^{-1}, dsDNA: 10 μg kg^{-1}, DOX: 6 mg kg^{-1}), and Ctrl (PBS). Each error bar shows the standard deviation of four independent measurements. Data are shown by mean and deviation. e,f) Data were also analyzed with ordinary one-way ANOVA. ****$p < 0.0001$.

immunohistochemical analysis. As shown in Figure 5c, dsDNA-contained NP groups (i.e., AN, MfAN, and MfAND) showed more effector T cells infiltration than the control group, which could be attributed to the dsDNA-mediated STING activation. Among them, MfAND group showed the highest performance in T cell infiltration, probably due to the synergistic effects of dsDNA-stimulated immunotherapy and DOX-mediated chemotherapy. The results in Figures 4d,e and 5 demonstrated that the designed NPs exhibited the antitumor immunity by inducing the production of IFN-β, by increasing effector T cell and enhancing effector T cell infiltration.

To demonstrate the general applicability of the STING-activating NPs for antitumor immunotherapy, we developed another tumor model by using 4T1 cells. As shown in **Figure 6**, the 4T1 tumor-xenografted mice were treated with the different NPs; very similar therapeutic results were obtained as for the B16F10 tumor model. MfD showed antitumor efficacy because of loaded DOX. All the three dsDNA-contained NPs (i.e., AN, MfAN, and MfAND groups) significantly inhibited the tumor growth. Among the three groups, the MfAND group showed the best outcome due to the synergistic effects of dsDNA-stimulated immunotherapy and DOX-mediated chemotherapy. We also explored the secondary effect model in Figure S14, Supporting Information. Again, among the three dsDNA-contained groups, the MfAND group showed the best outcome on the contralateral model, which was consistent with reported studies.[41,42]

3. Conclusion

In summary, we have designed and synthesized the multifunctional STING-activating NPs for synergistic antitumor immunotherapy. We showed that all the dsDNA-contained NPs successfully activated the STING pathway by inducing the production of IFN-β, by increasing T cell priming and enhancing effector T cell infiltration. More excitingly, when injected intravenously in tumor-bearing mice, the dsDNA-contained NPs accumulated in tumors via EPR effect, effectively inhibited the tumor growth, and prolonged the survival rate. Among the dsDNA-contained NPs, the MfAND showed the high antitumor efficacy both in vitro and in vivo, validating the synergistic therapeutic effect of the dsDNA-stimulated immunotherapy and DOX-mediated chemotherapy. In addition, we noted that there was a detectable antitumor activity in Mf group for both tumor models (Figures 4a and 6a). It is known that Mn_3O_4 NPs have catalase-mimicking activity and could act as an oxygenerator to produce O_2 from H_2O_2.[43,44] On the other hand, hypoxia, one of the prominent features of tumor microenvironment,[45,46] has been regarded as an important factor in immunosuppression.[47,48] Therefore, we hypothesized that the in situ generated O_2 by Mf in the tumors would improve the tumor hypoxia and benefit the immunotherapy. To demonstrate our hypothesis, first we investigated the catalase-mimicking activity of Mf. As shown in Figure S15, Supporting Information, the Mf NPs exhibited good

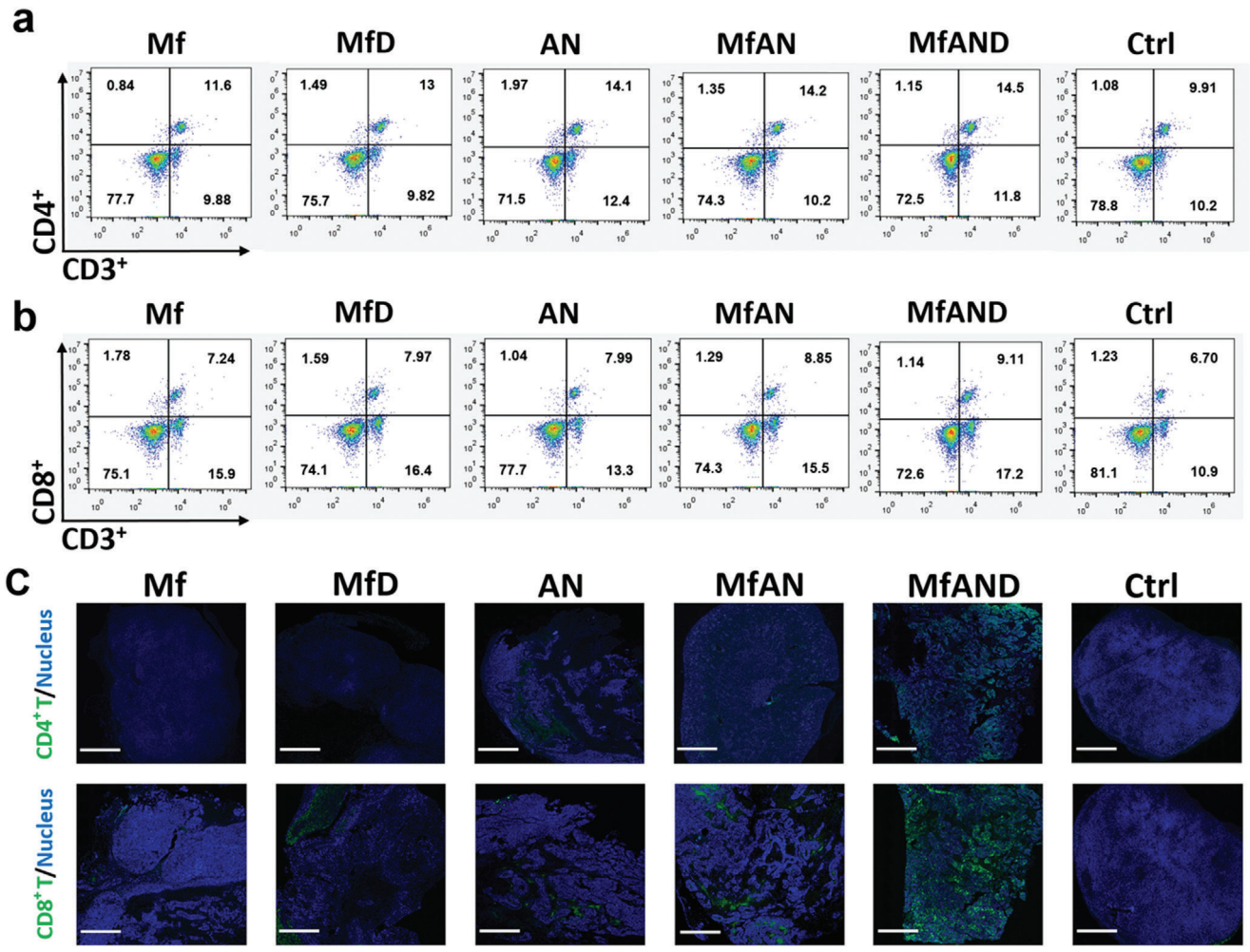

Figure 5. Mechanism analysis of antitumor activity of the designed NPs. a,b) Flow cytometry of $CD4^+$ and $CD8^+$ T cells in spleen, respectively. c) Immunohistochemical analysis of $CD4^+$ and $CD8^+$ T cells in dissected tumors, respectively. Indicated groups: Mf (Mn_3O_4, 5 mg kg^{-1}), MfD (Mn_3O_4: 5 mg kg^{-1}, DOX: 6 mg kg^{-1}), AN (dsDNA: 10 μg kg^{-1}), MfAN (Mn_3O_4: 5 mg kg^{-1}, dsDNA: 10 μg kg^{-1}), MfAND (Mn_3O_4: 5 mg kg^{-1}, dsDNA: 10 μg kg^{-1}, DOX: 6 mg kg^{-1}), and Ctrl (PBS). Scale bar: 1000 μm.

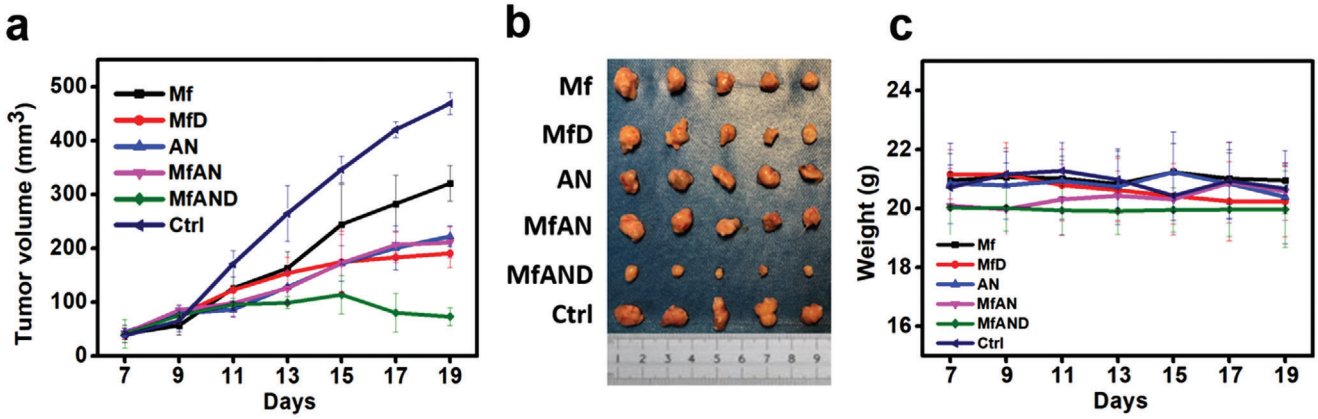

Figure 6. Antitumor effect of the NPs on 4T1 xenograft tumor. a) Tumor volume changes, b) corresponding tumor images, and c) body weight changes of 4T1 tumor-bearing mice after the indicated treatments. Indicated treatments: Mf (Mn_3O_4: 5 mg kg^{-1}), MfD (Mn_3O_4: 5 mg kg^{-1}, DOX: 6 mg kg^{-1}), AN (dsDNA: 10 μg kg^{-1}), MfAN (Mn_3O_4: 5 mg kg^{-1}, dsDNA: 10 μg kg^{-1}), MfAND (Mn_3O_4: 5 mg kg^{-1}, dsDNA: 10 μg kg^{-1}, DOX: 6 mg kg^{-1}) and Ctrl (PBS). Each error bar shows the standard deviation of four independent measurements.

catalase-mimicking activity by converting H_2O_2 into O_2. We then explored whether Mf could benefit the hypoxia improvement in vitro by using deferoxamine (DFO) as a hypoxia inducer. As shown in Figure S16, Supporting Information, Mf effectively relieved the hypoxia. Hypoxia-induced factor 1α (HIF-1α) is the direct regulator of hypoxia in tumor. Thus, we detected the HIF-1α expression in tumor tissues by immunohistochemical analysis (Figure S17, Supporting Information). The expression of HIF-1α decreased in all the Mf-contained groups. These results indicated that the catalase-mimicking Mf might benefit the antitumor immunotherapy by overcoming the hypoxia in tumor microenvironment, the exact mechanism is still under investigation.

The current strategy is conceptually novel and advantageous in several aspects: First, this is the first demonstration of NP-enabled delivery of dsDNA as a STING agonist for STING-mediated antitumor immunotherapy. Second, co-delivery of chemical drug and STING activator achieved the synergistic antitumor therapy based on the self-assembled NPs. Last, the NPs were multifunctional and tumor microenvironment responsive. The NPs were decomposed in tumor area and released chemical drug/STING activator for therapy, meanwhile the in situ generated oxygen improved hypoxia and released Mn ion functioned for MRI imaging. With the quick development of STING-mediated signal pathway and the well-established nanomedicine, we anticipate that the combination of the newly elucidated immunity mechanisms (such as STING-associated phagocytosis, senescence, and antitumor activity) with innovative nanotechnologies (such as the one developed here) will benefit the further cancer immunotherapy as well as other related diseases.[25,49,50]

4. Experimental Section

Chemicals and Materials: Potassium permanganate ($KMnO_4$), H_2O_2 (30%), GSH, sodium citrate, ethanol, and oleic acid were obtained from Sinopharm Chemical Reagent Co., Ltd. (Shanghai, China). Chloroauric acid ($HAuCl_4{\cdot}3H_2O$) was purchased from Sigma-Aldrich (St. Louis, MO, USA). Reagents for cell culture, including fetal bovine serum (FBS), PBS, high glucose Dulbecco's modified Eagle's medium (DMEM), trypsin solution, penicillin, and streptomycin, were from Thermo Fisher Scientific (China). All antibodies were from BD Bioscience (R&D Systems Co., Ltd.). Mouse IFN-β detection kit and TNF-α detection kit were provided by BD Bioscience. 59-nt poly(dT) ssDNA modified with HS-SH C6 at 3′ end and 59-nt poly(dA) ssDNA were synthesized by Sangon Biotech Co., Ltd. (Shanghai, China).

Cell Strains: B16F10 (murine melanoma cell), 4T1 (murine mammary cancer cell), and RAW 264.7 (leukemia cells in mouse macrophage) cells were supplied by ATCC. CCK-8 kit was purchased from DOJINDO (Kumamoto, Japan), nuclear dye Hochest 33342 was from Sangon Biotech (Shanghai, China), and hypoxia detection kit was from Enzo Life Science, Inc. (NY, USA). All reagents were used as received without further purification. Deionized water was used in all experiments (18.2 MΩ cm, Millipore).

Instrumentation: SEM images were obtained by Zeiss Ultra 55 scanning electron microscope operating at 3 kV. TEM images were obtained by EOL JEM-2100 transmission electron microscope with an acceleration voltage of 200 kV. UV–vis absorption spectra were measured by a spectrophotometer (UV-3600 Plus, Shimadzu, Japan). Absorption values of microplates were collected by SpectraMax M2/M2e (Molecular Devices, USA). Dynamic lighting scattering and zeta-potential distribution were measured by a Nanosizer ZS90 (Malvern Zetasizer, Malvern). MRI was performed on a 7.0 T small animal MR scanner (Bruker PharmaScan, Germany).

Synthesis of Mn_3O_4: Mn_3O_4 nanoflower (Mf) was synthesized according to a previous procedure.[32,33] Briefly, 1.0 g of $KMnO_4$ was dissolved in 500 mL of water and then stirred for 30 min. A total of 10.0 mL of oleic acid was added to the $KMnO_4$ solution. The solution was stirred for about 5 h at the room temperature until the color changed from modena to brown-black. The brown-black product was collected and washed with deionized water and ethanol for three times each. The product was then dried at 80 °C for 10 h to get the precursor, which was calcined at 200 °C for 5 h to obtain monodispersed Mf.

Synthesis of Au-dsDNA: Gold NPs (AuNPs) were prepared by using the citrate reduction method.[31] AuNPs conjugated with thiolated-ssDNA (Au-ssDNA) were prepared by a salt-aging procedure.[34] In brief, 100 µL of AuNPs stock solution was incubated with thiolated-ssDNA (59-nt poly(dT)) overnight. NaCl was slowly added to increase ionic strength every 12 h until the final NaCl concentration was 0.15 M. Au-ssDNA was collected and resuspended in 10×10^{-3} M at pH 7.4 phosphate buffer (containing 0.15 M NaCl). Au-dsDNA (i.e., AN) was obtained by annealing the Au-ssDNA and the complementary ssDNA (59-nt poly(dA)), and stored in 4 °C for later use.

Synthesis of MfAN and MfAND: MfAN and MfAND were freshly prepared before use. AN and Mf were incubated for 10 min with weak sonication to get MfAN. MfAND was obtained by mixing DOX with MfAN.

Cell Culture and Cytotoxicity Analysis: B16F10, 4T1, and RAW 264.7 cells were cultured with 10% FBS and high glucose DMEM at 37 °C in a 5% CO_2 incubator. For cytotoxicity analysis, cells were subcultured overnight into 96-well plates at a density of 8×10^3 cells per well. Next day, cells were treated with NPs with appropriate concentrations. After the treatments, cell counting kit-8 (CCK-8) assay was used to assess the cell viability.

Improvement of Hypoxia Microenvironment: Oxygen generation ability of Mf was detected by a hypoxia detection kit in vitro. Cells were subcultured into a confocal culture dish. Next day, the cells were washed three times with PBS, incubated with 5 µg mL^{-1} Mf for 4 h, and refreshed with the culture medium containing hypoxia detection reagent and hypoxia inducer DFO (200×10^{-6} M final concentration) for 3.5 h (normal culture condition at 37 °C in 5% CO_2 incubator). Later, the cells were gently washed three times with PBS, fixed, and stained with nuclei dye Hochest 33342. Finally, cell imaging was obtained by confocal laser scanning microscopy (CLSM, IX-83, Olympus and Andor). Hypoxia probe: EX/EM 570 nm/596 nm, Hochest 33342: EX/EM 350 nm/460 nm.

Phagocytosis In Vitro: First, B16F10 cells were subcultured overnight into six-well plates with 3×10^5 seeding density. When the confluency was up to 70%, cells were treated with the following groups: Mf (Mn_3O_4: 5 µg mL^{-1}), MfD (Mn_3O_4: 5 µg mL^{-1}, DOX: 125×10^{-9} M), AN (dsDNA: 6 µg mL^{-1}), MfAN (Mn_3O_4: 5 µg mL^{-1}, dsDNA: 6 µg mL^{-1}), MfAND (Mn_3O_4: 5 µg mL^{-1}, dsDNA: 6 µg mL^{-1}, DOX: 125×10^{-9} M), and Ctrl (PBS). After these treatments, the culture supernatant of B16F10 cells was collected for IFN-β detection. Meanwhile these treated B16F10 cells were placed under the UV radiation to kill all the cells. Later, these dying B16F10 cells were fed to RAW 264.7 cells. After the phagocytosis of dying B16F10 cells, the culture supernatant of RAW 264.7 cells was collected and prepared for IFN-β detection.

Ability of Antivirus In Vitro: To detect the antiviral ability, B16F10 and RAW 264.7 cells were seeded overnight into six-well plates at a density of 3×10^5 per well. When the confluency was up to 50%, cells were washed and infected with adenovirus of expression green fluorescence protein (multiplicity of infection = 30). The cells were refreshed with new culture medium after 6 h of infection. After 24 h, cells were imaged with a fluorescence microscope (Jiangnanyongxin Corporation, Nanjing, China).

Tumor Model In Vivo: For antitumor model, C57BL/6 mice (male, 4–6 week, ≈20 g) were purchased from Nanjing Medical University and raised in a specific pathogen-free environment. B16F10 cells were harvested and then transplanted intradermally to the right flank of mice with the density of 5×10^5 cells per mouse. When the volume of tumor reached 50 mm^3 (volume calculated according the formula V = length × width × width/2, the length and width of tumor were measured by digital calipers), mice were separated into six groups with randomization, and treated with designed NPs by intravenous injection every 2 days. Six treatment groups were as follow: Mf (Mn_3O_4: 5 mg kg^{-1}), MfD (Mn_3O_4: 5 mg kg^{-1}, DOX:

mg kg^{-1}), AN (dsDNA: 10 μg kg^{-1}), MfAN (Mn_3O_4: 5 mg kg^{-1}, dsDNA: 10 μg kg^{-1}), MfAND (Mn_3O_4: 5 mg kg^{-1}, dsDNA: 10 μg kg^{-1}, DOX: 6 mg kg^{-1}), and Ctrl (PBS). Mice were sacrificed when tumor volume was more than 2000 mm^3.

For survival model, C57BL/6 mice (male, 4–6 week, ≈20 g) were transplanted intradermally with tumor cells as the above. Later, the mice were randomized into six groups with the same treatments as the antitumor model. Mice were intravenously injected with designed NPs three times at days 7, 9, and 11, respectively. When tumor volume was more than 2000 mm^3, mice were sacrificed.

All the animal studies were approved by the Committee for Experimental Animals Welfare and Ethics of Nanjing Drum Tower Hospital, the Affiliated Hospital of Nanjing University Medical School.

Quantification of Cytokines in Serum of Peripheral Blood: Peripheral blood was collected at 0, 3, 6, and 9 h after NPs treatment. Indicated groups were Mf (Mn_3O_4: 5 mg kg^{-1}), MfD (Mn_3O_4: 5 mg kg^{-1}, DOX: 6 mg kg^{-1}), AN (dsDNA: 10 μg kg^{-1}), MfAN (Mn_3O_4: 5 mg kg^{-1}, dsDNA: 10 μg kg^{-1}), MfAND (Mn_3O_4: 5 mg kg^{-1}, dsDNA: 10 μg kg^{-1}, DOX: 6 mg kg^{-1}), and Ctrl (PBS). Blood was left at room temperature for 20 min to clot and then centrifuged to obtain serum. The levels of IFN-β and TNF-α were detected by mouse IFN-β and TNF-α enzyme-linked immunosorbent assay kits, respectively, operated according to the standard manuals.

Immunohistochemical Analysis of Dissected Tumor: The dissected tumors were acquired after the indicated treatments, and then were mounted with OCT compound. Five micrometer slices were separated by microtone and imaged by CLSM after series of blocking-washing-staining standard procedures.

Quantitative Analysis of Effector T Cells in Spleen: Mice were sacrificed for spleens after indicated treatments. Fresh spleens were washed with PBS three times and later were carefully grinded with syringe's rubber end to get cell suspension. Cell suspensions were treated with red blood cell lysis buffer (Beyotime Institute of Biotechnology, Shanghai, China), centrifuged, and washed at least three times. The 1×10^6 cells of each treatment were prepared for flow cytometry analysis through series of blocking-washing-staining procedures according to standard protocols. Note that all the procedures should be operated in a sterile environment.

Supporting Information

Supporting Information is available from the Wiley Online Library or from the author.

Acknowledgements

The authors thank Chao Zhang, Bin Li, Wen Cao, Yixuan Li, Liming Zheng, Wenli Diao, Xiaozhi Zhao, and Quan Wang for their help with experiments. This work was supported by National Natural Science Foundation of China (91859112, 21722503, and 21874067), Natural Science Foundation of Jiangsu Province (BK20180340), 973 Program (2015CB659400), PAPD program, Shuangchuang Program of Jiangsu Province, Open Funds of the State Key Laboratory of Analytical Chemistry for Life Science (SKLACLS1704), Open Funds of the State Key Laboratory of Coordination Chemistry (SKLCC1819), and Fundamental Research Funds for the Central Universities (021314380145).

Conflict of Interest

M.Z. and H.W. are the authors of patent application. Rests of the authors declare no conflict of interest.

Keywords

cancer immunotherapy, DNA nanotechnology, immunosuppression, STING activation, synergistic antitumor therapy

Received: January 12, 2020
Revised: May 8, 2020
Published online: June 2, 2020

[1] A. Ribas, J. D. Wolchok, *Science* **2018**, *359*, 1350.
[2] P. Gotwals, S. Cameron, D. Cipolletta, V. Cremasco, A. Crystal, B. Hewes, B. Mueller, S. Quaratino, C. Sabatos-Peyton, L. Petruzzelli, J. A. Engelman, G. Dranoff, *Nat. Rev. Cancer* **2017**, *17*, 286.
[3] C. Pfirschke, C. Engblom, S. Rickelt, V. Cortez-Retamozo, C. Garris, F. Pucci, T. Yamazaki, V. Poirier-Colame, A. Newton, Y. Redouane, Y.-J. Lin, G. Wojtkiewicz, Y. Iwamoto, M. Mino-Kenudson, T. G. Huynh, R. O. Hynes, G. J. Freeman, G. Kroemer, L. Zitvogel, R. Weissleder, M. J. Pittet, *Immunity* **2016**, *44*, 343.
[4] Y. Yang, Y. Lu, P. L. Abbaraju, J. Zhang, M. Zhang, G. Xiang, C. Yu, *Angew. Chem., Int. Ed.* **2017**, *56*, 8446.
[5] Z. Wang, Y. Fu, Z. Kang, X. Liu, N. Chen, Q. Wang, Y. Tu, L. Wang, S. Song, D. Ling, H. Song, X. Kong, C. Fan, *J. Am. Chem. Soc.* **2017**, *139*, 15784.
[6] G. Lan, K. Ni, Z. Xu, S. S. Veroneau, Y. Song, W. Lin, *J. Am. Chem. Soc.* **2018**, *140*, 5670.
[7] C. Wang, Y. Ye, Q. Hu, A. Bellotti, Z. Gu, *Adv. Mater.* **2017**, *29*, 1606036.
[8] Y. Mi, C. C. Smith, F. Yang, Y. Qi, K. C. Roche, J. S. Serody, B. G. Vincent, A. Z. Wang, *Adv. Mater.* **2018**, *30*, 1706098.
[9] Q. Chen, L. Xu, C. Liang, C. Wang, R. Peng, Z. Liu, *Nat. Commun.* **2016**, *7*, 13193.
[10] E. J. Sayour, A. Grippin, G. De Leon, B. Stover, M. Rahman, A. Karachi, B. Wummer, G. Moore, P. Castillo-Caro, K. Fredenburg, M. R. Sarkisian, J. Huang, L. P. Deleyrolle, B. Sahay, S. Carrera-Justiz, H. R. Mendez-Gomez, D. A. Mitchell, *Nano Lett.* **2018**, *18*, 6195.
[11] Y. Ye, C. Wang, X. Zhang, Q. Hu, Y. Zhang, Q. Liu, D. Wen, J. Milligan, A. Bellotti, L. Huang, G. Dotti, Z. Gu, *Sci. Immunol.* **2017**, *2*, eaan5692.
[12] M. Konstantinidou, T. Zarganes-Tzitzikas, K. Magiera-Mularz, T. A. Holak, A. Dömling, *Angew. Chem., Int. Ed.* **2018**, *57*, 4840.
[13] J. Galon, D. Bruni, *Nat. Rev. Drug Discovery* **2019**, *18*, 197.
[14] X. Duan, C. Chan, W. Lin, *Angew. Chem., Int. Ed.* **2019**, *58*, 670.
[15] C. S. Hinrichs, S. A. Rosenberg, *Immunol. Rev.* **2014**, *257*, 56.
[16] Q. Chen, Q. Hu, E. Dukhovlinova, G. Chen, S. Ahn, C. Wang, E. A. Ogunnaike, F. S. Ligler, G. Dotti, Z. Gu, *Adv. Mater.* **2019**, *31*, 1900192.
[17] G. N. Barber, *Nat. Rev. Immunol.* **2015**, *15*, 760.
[18] J. Ahn, D. Gutman, S. Saijo, G. N. Barber, *Proc. Natl. Acad. Sci. USA* **2012**, *109*, 19386.
[19] H. Ishikawa, G. N. Barber, *Nature* **2008**, *455*, 674.
[20] H. Ishikawa, Z. Ma, G. N. Barber, *Nature* **2009**, *461*, 788.
[21] B. Zhong, Y. Yang, S. Li, Y.-Y. Wang, Y. Li, F. Diao, C. Lei, X. He, L. Zhang, P. Tien, H.-B. Shu, *Immunity* **2008**, *29*, 538.
[22] J. Wu, L. Sun, X. Chen, F. Du, H. Shi, C. Chen, Z. J. Chen, *Science* **2013**, *339*, 826.
[23] L. Li, Q. Yin, P. Kuss, Z. Maliga, J. L. Millán, H. Wu, T. J. Mitchison, *Nat. Chem. Biol.* **2014**, *10*, 1043.
[24] J. M. Ramanjulu, G. S. Pesiridis, J. Yang, N. Concha, R. Singhaus, S.-Y. Zhang, J.-L. Tran, P. Moore, S. Lehmann, H. C. Eberl, M. Muelbaier, J. L. Schneck, J. Clemens, M. Adam, J. Mehlmann, J. Romano, A. Morales, J. Kang, L. Leister, T. L. Graybill, A. K. Charnley, G. Ye, N. Nevins, K. Behnia, A. I. Wolf, V. Kasparcova, K. Nurse, L. Wang, Y. Li, M. Klein, C. B. Hopson, J. Guss, M. Bantscheff, G. Bergamini, M. A. Reilly, Y. Lian, K. J. Duffy, J. Adams, K. P. Foley, P. J. Gough, R. W. Marquis, J. Smothers, A. Hoos, J. Bertin, *Nature* **2018**, *564*, 439.
[25] M. Luo, H. Wang, Z. Wang, H. Cai, Z. Lu, Y. Li, M. Du, G. Huang, C. Wang, X. Chen, M. R. Porembka, J. Lea, A. E. Frankel, Y.-X. Fu, Z. J. Chen, J. Gao, *Nat. Nanotechnol.* **2017**, *12*, 648.

[26] J. Ahn, T. Xia, A. Rabasa Capote, D. Betancourt, G. N. Barber, *Cancer Cell* **2018**, *33*, 862.
[27] L. A. Emens, G. Middleton, *Cancer Immunol. Res.* **2015**, *3*, 436.
[28] S. Cornen, E. Vivier, *Science* **2018**, *362*, 1355.
[29] R. A. Lake, B. W. S. Robinson, *Nat. Rev. Cancer* **2005**, *5*, 397.
[30] P. Kadiyala, D. Li, F. M. Nuñez, D. Altshuler, R. Doherty, R. Kuai, M. Yu, N. Kamran, M. Edwards, J. J. Moon, P. R. Lowenstein, M. G. Castro, A. Schwendeman, *ACS Nano* **2019**, *13*, 1365.
[31] Y. Hu, H. Cheng, X. Zhao, J. Wu, F. Muhammad, S. Lin, J. He, L. Zhou, C. Zhang, Y. Deng, P. Wang, Z. Zhou, S. Nie, H. Wei, *ACS Nano* **2017**, *11*, 5558.
[32] H. Chen, J. He, *J. Phys. Chem. C* **2008**, *112*, 17540.
[33] N. Singh, M. A. Savanur, S. Srivastava, P. D'Silva, G. Mugesh, *Angew. Chem., Int. Ed.* **2017**, *56*, 14267.
[34] B. Liu, Z. Huang, J. Liu, *Angew. Chem., Int. Ed.* **2018**, *57*, 9439.
[35] O. Demaria, A. De Gassart, S. Coso, N. Gestermann, J. Di Domizio, L. Flatz, O. Gaide, O. Michielin, P. Hwu, T. V. Petrova, F. Martinon, R. L. Modlin, D. E. Speiser, M. Gilliet, *Proc. Natl. Acad. Sci. USA* **2015**, *112*, 15408.
[36] T. Xia, H. Konno, G. N. Barber, *Cancer Res.* **2016**, *76*, 6747.
[37] V. Bronte, *Immunity* **2014**, *41*, 679.
[38] T. Nakamura, H. Miyabe, M. Hyodo, Y. Sato, Y. Hayakawa, H. Harashima, *J. Controlled Release* **2015**, *216*, 149.
[39] S. T. Koshy, A. S. Cheung, L. Gu, A. R. Graveline, D. J. Mooney, *Adv. Biosyst.* **2017**, *1*, 1600013.
[40] J. R. Baird, D. Friedman, B. Cottam, T. W. Dubensky, D. B. Kanne, S. Bambina, K. Bahjat, M. R. Crittenden, M. J. Gough, *Cancer Res.* **2016**, *76*, 50.
[41] Y. Liu, W. N. Crowe, L. Wang, Y. Lu, W. J. Petty, A. A. Habib, D. Zhao, *Nat. Commun.* **2019**, *10*, 5108.
[42] S. Chattopadhyay, Y.-H. Liu, Z.-S. Fang, C.-L. Lin, J.-C. Lin, B.-Y. Yao, C.-M. J. Hu, *Nano Lett.* **2020**, *20*, 2246.
[43] J. Yao, Y. Cheng, M. Zhou, S. Zhao, S. Lin, X. Wang, J. Wu, S. Li, H. Wei, *Chem. Sci.* **2018**, *9*, 2927.
[44] J. Wu, X. Wang, Q. Wang, Z. Lou, S. Li, Y. Zhu, L. Qin, H. Wei, *Chem. Soc. Rev.* **2019**, *48*, 1004.
[45] W.-L. Liu, T. Liu, M.-Z. Zou, W.-Y. Yu, C.-X. Li, Z.-Y. He, M.-K. Zhang, M.-D. Liu, Z.-H. Li, J. Feng, X.-Z. Zhang, *Adv. Mater.* **2018**, *30*, 1802006.
[46] M. Li, J. Xia, R. Tian, J. Wang, J. Fan, J. Du, S. Long, X. Song, J. W. Foley, X. Peng, *J. Am. Chem. Soc.* **2018**, *140*, 14851.
[47] S. Chouaib, M. Z. Noman, K. Kosmatopoulos, M. A. Curran, *Oncogene* **2017**, *36*, 439.
[48] S. K. Daniel, K. M. Sullivan, K. P. Labadie, V. G. Pillarisetty, *Clin. Transl. Med.* **2019**, *8*, 10.
[49] T. Li, Z. J. Chen, *J. Exp. Med.* **2018**, *215*, 1287.
[50] J. Nassour, R. Radford, A. Correia, J. M. Fusté, B. Schoell, A. Jauch, R. J. Shaw, J. Karlseder, *Nature* **2019**, *565*, 659.